



**HAL**  
open science

## First principles study on the lattice thermal conductivity of $\alpha$ -phase Ga<sub>2</sub>O<sub>3</sub>

Gang Yang, Pedro Rojo Romeo, Aleksandra Apostoluk, Bertrand Vilquin

► **To cite this version:**

Gang Yang, Pedro Rojo Romeo, Aleksandra Apostoluk, Bertrand Vilquin. First principles study on the lattice thermal conductivity of  $\alpha$ -phase Ga<sub>2</sub>O<sub>3</sub>. *Journal of Vacuum Science & Technology A*, 2022, 40 (5), pp.052801. 10.1116/6.0001870 . hal-03735982

**HAL Id: hal-03735982**

**<https://hal.science/hal-03735982>**

Submitted on 3 Dec 2022

**HAL** is a multi-disciplinary open access archive for the deposit and dissemination of scientific research documents, whether they are published or not. The documents may come from teaching and research institutions in France or abroad, or from public or private research centers.

L'archive ouverte pluridisciplinaire **HAL**, est destinée au dépôt et à la diffusion de documents scientifiques de niveau recherche, publiés ou non, émanant des établissements d'enseignement et de recherche français ou étrangers, des laboratoires publics ou privés.



Distributed under a Creative Commons Attribution 4.0 International License

# First principles study on the lattice thermal conductivity of $\alpha$ -phase $\text{Ga}_2\text{O}_3$

Cite as: J. Vac. Sci. Technol. A **40**, 052801 (2022); <https://doi.org/10.1116/6.0001870>

Submitted: 18 March 2022 • Accepted: 23 June 2022 • Published Online: 21 July 2022

Gang Yang, Pedro Rojo Romeo, Aleksandra Apostoluk, et al.

## COLLECTIONS

Paper published as part of the special topic on [Gallium Oxide Materials and Devices](#)



View Online



Export Citation



CrossMark

## ARTICLES YOU MAY BE INTERESTED IN

[A review of  \$\text{Ga}\_2\text{O}\_3\$  materials, processing, and devices](#)

Applied Physics Reviews **5**, 011301 (2018); <https://doi.org/10.1063/1.5006941>

[\$\beta\$ -Gallium oxide power electronics](#)

APL Materials **10**, 029201 (2022); <https://doi.org/10.1063/5.0060327>

[A review of band structure and material properties of transparent conducting and semiconducting oxides:  \$\text{Ga}\_2\text{O}\_3\$ ,  \$\text{Al}\_2\text{O}\_3\$ ,  \$\text{In}\_2\text{O}\_3\$ ,  \$\text{ZnO}\$ ,  \$\text{SnO}\_2\$ ,  \$\text{CdO}\$ ,  \$\text{NiO}\$ ,  \$\text{CuO}\$ , and  \$\text{Sc}\_2\text{O}\_3\$](#)

Applied Physics Reviews **9**, 011315 (2022); <https://doi.org/10.1063/5.0078037>





**HIDEN**  
ANALYTICAL



40  
YEARS  
1982 - 2022

## Instruments for Advanced Science

- Knowledge,
- Experience,
- Expertise

Click to view our product catalogue

Contact Hiden Analytical for further details:  
[www.HidenAnalytical.com](http://www.HidenAnalytical.com)  
[info@hideninc.com](mailto:info@hideninc.com)

Gas Analysis



- ▶ dynamic measurement of reaction gas streams
- ▶ catalysis and thermal analysis
- ▶ molecular beam studies
- ▶ dissolved species probes
- ▶ fermentation, environmental and ecological studies

Surface Science



- ▶ UHVTPD
- ▶ SIMS
- ▶ end point detection in ion beam etch
- ▶ elemental imaging - surface mapping

Plasma Diagnostics



- ▶ plasma source characterization
- ▶ etch and deposition process reaction kinetic studies
- ▶ analysis of neutral and radical species

Vacuum Analysis



- ▶ partial pressure measurement and control of process gases
- ▶ reactive sputter process control
- ▶ vacuum diagnostics
- ▶ vacuum coating process monitoring

# First principles study on the lattice thermal conductivity of $\alpha$ -phase $\text{Ga}_2\text{O}_3$

Cite as: J. Vac. Sci. Technol. A 40, 052801 (2022); doi: 10.1116/6.0001870

Submitted: 18 March 2022 · Accepted: 23 June 2022 ·

Published Online: 21 July 2022



Gang Yang, Pedro Rojo Romeo, Aleksandra Apostoluk, and Bertrand Vilquin<sup>a)</sup>

## AFFILIATIONS

Université de Lyon, Ecole Centrale de Lyon, INSA Lyon, UCBL, CPE Lyon, CNRS, INL UMR5270, 69130 Ecully, France

**Note:** This paper is part of the Special Topic Collection on Gallium Oxide Materials and Devices.

<sup>a)</sup>Author to whom correspondence should be addressed: [bertrand.vilquin@ec-lyon.fr](mailto:bertrand.vilquin@ec-lyon.fr)

## ABSTRACT

In this article, lattice thermal conductivity of  $\alpha$ -phase  $\text{Ga}_2\text{O}_3$  is investigated in a way of combining the first principles calculation and iterative solving the Boltzmann transport equation. Real-space displacement approach is employed in order to obtain both second- and third-order force constants. The effect of the microstructure on lattice thermal conductivity of  $\alpha$ -phase  $\text{Ga}_2\text{O}_3$  has been extensively studied and widely discussed. The results indicate that  $\alpha$ -phase  $\text{Ga}_2\text{O}_3$  exhibit a lower thermal conductivity compared with  $\beta$ -phase  $\text{Ga}_2\text{O}_3$  in a temperature range from 30 to 800 K. At room temperature, 300 K, the calculated thermal conductivities of  $\alpha$ -phase  $\text{Ga}_2\text{O}_3$  are 11.61, 9.38, and  $8.94 \text{ Wm}^{-1} \text{ K}^{-1}$  in the directions [100], [010], and [001], respectively. The lower thermal conductivity of  $\alpha$ -phase  $\text{Ga}_2\text{O}_3$  can be attributed to the mass difference and bond strength between Ga and O atoms. As for the phonon transport analysis, it is related to the three phonon scattering mechanism. Compared with  $\beta$ -phase  $\text{Ga}_2\text{O}_3$ ,  $\alpha$ -phase  $\text{Ga}_2\text{O}_3$  exhibits a higher anharmonic phonon scattering rate. Our study aims to help to understand the thermal transport mechanism of  $\alpha$ -phase  $\text{Ga}_2\text{O}_3$  material and provide useful guidance for the future device applications and enrich the existing state of the art.

© 2022 Author(s). All article content, except where otherwise noted, is licensed under a Creative Commons Attribution (CC BY) license (<http://creativecommons.org/licenses/by/4.0/>). <https://doi.org/10.1116/6.0001870>

## I. INTRODUCTION

Wide-bandgap semiconductors, which refer to semiconductor materials with a larger bandgap than conventional semiconductors, represent a stimulating and challenging area of research in materials for optoelectronics.<sup>1</sup> In the last decade, gallium oxide ( $\text{Ga}_2\text{O}_3$ ) has attracted a lot of attention as a promising wide-bandgap semiconductor. The material properties of  $\text{Ga}_2\text{O}_3$  have been widely investigated and fabrication or preparation technologies for  $\text{Ga}_2\text{O}_3$  materials have been rapidly developed.<sup>2–4</sup> Similar to other polymorphic sesquioxide systems, such as  $\text{In}_2\text{O}_3$  and  $\text{Al}_2\text{O}_3$ ,  $\text{Ga}_2\text{O}_3$  can form five different polymorphs known as  $\alpha$ ,  $\beta$ ,  $\gamma$ ,  $\delta$ , and  $\epsilon$ .<sup>5</sup> Among them,  $\beta$ -phase is the most stable and widely used in semiconductor industry. However, along with advanced deposited technology emergence, corundum-structured  $\alpha$ - $\text{Ga}_2\text{O}_3$  crystal thin films were successfully grown or deposited on various substrates.<sup>6–11</sup> Specifically, in recent years, material properties of  $\alpha$ - $\text{Ga}_2\text{O}_3$  have

received growing attention in both academic research and industrial applications.<sup>12–14</sup>

Compared to other wide-bandgap semiconductor materials, such as SiC and GaN,  $\text{Ga}_2\text{O}_3$  has a relative low thermal conductivity of about  $16\text{--}21 \text{ Wm}^{-1} \text{ K}^{-1}$  at room temperature for  $\beta$ -phase.<sup>15</sup> In contrast, thermal conductivities of SiC and GaN are reported as high as 380 and  $220 \text{ Wm}^{-1} \text{ K}^{-1}$  at room temperature, respectively.<sup>16,17</sup> For  $\text{Ga}_2\text{O}_3$ -based high-power electrical devices, a low thermal conductivity will significantly affect the device performance, reliability, as well as the safety.<sup>18</sup> Moreover, thermal properties of  $\text{Ga}_2\text{O}_3$  materials are not only important for electrical devices, but also critical for a substrate temperature control, as well as uniformity during the epitaxial growth or other physical and chemical vapor deposition process. Currently, various growth techniques (e.g., molecular beam epitaxy, halide vapor phase epitaxy, and chemical vapor deposition) have been developed to directly

synthesize polymorph  $\text{Ga}_2\text{O}_3$  thin films.<sup>2</sup> In particular, various phases of gallium oxide films can be obtained at the same time using the RF magnetron sputtering process as the obtained phases depend on the substrate planes and deposition parameters, such as the temperature.<sup>19</sup> Therefore, a detailed characterization of individual physical properties of each  $\text{Ga}_2\text{O}_3$  phase is of primordial importance, especially,  $\alpha$ -phase and  $\beta$ -phase  $\text{Ga}_2\text{O}_3$  can be distinguished during the deposition process at various temperatures.

Previous studies on the thermal conductivity of  $\text{Ga}_2\text{O}_3$  mainly focused on the common  $\beta$ -phase, and the experimental measurements were made mostly using the  $2\omega$ ,  $3\omega$  methods as well as time domain thermoreflectance technique.<sup>20–22</sup> Recently, Raman thermometry technology was employed to investigate the thermal conductivity of  $\beta$ - $\text{Ga}_2\text{O}_3$  nanomembrane and thin films.<sup>23,24</sup> These experimental results show a significant anisotropy of the thermal conductivity for  $\beta$ -phase  $\text{Ga}_2\text{O}_3$  materials. However, thermal conductivity of other phases of  $\text{Ga}_2\text{O}_3$ , such as  $\alpha$  and  $\epsilon$  phases, still needs to be studied and explored.

In recent years, first principles calculations in condensed matter physics and materials science have attracted a lot of interest and were widely used to predict thermal transport properties of various materials, especially when phonon-based calculations became routine.<sup>25</sup> Harmonic force constants (second-order force constants) can be obtained from total energy calculations based on the density functional theory (DFT). In addition, some state-of-the-art modeling has also been developed to derive the anharmonic force constants (third-order force constants) from the first principles calculation.<sup>26</sup> Knowing both second-order and third-order force constants can permit us to directly solve the phonon Boltzmann transport equation and obtain lattice thermal conductivity. Previously, Liu *et al.* studied lattice dynamic and thermodynamic properties of  $\beta$ - $\text{Ga}_2\text{O}_3$  from first principles calculations.<sup>27</sup> Santia *et al.* investigated lattice thermal conductivity of monoclinic  $\beta$ - $\text{Ga}_2\text{O}_3$  from first principles calculation.<sup>15</sup> Mu *et al.* implemented *ab initio* study on enhanced thermal conductivity in ordered  $\text{AlGaO}_3$  alloys.<sup>28</sup> Yan *et al.* studied the phonon mode contributions to lattice thermal conductivity of pristine and defective  $\beta$ - $\text{Ga}_2\text{O}_3$  using first-principles calculations.<sup>29</sup> However, all above investigation mainly focus on the  $\beta$ -phase of  $\text{Ga}_2\text{O}_3$ . There are no studies or reports on the lattice thermal conductivity of corundum-structured  $\alpha$ - $\text{Ga}_2\text{O}_3$  material.<sup>30</sup> Hence, a theoretical study on the lattice thermal conductivity of  $\alpha$ - $\text{Ga}_2\text{O}_3$  is necessary.

The principal objective of the present research is to examine the phonon thermal transport mechanism for  $\alpha$ - $\text{Ga}_2\text{O}_3$  materials. The effects of the microstructure on the lattice thermal conductivity have been investigated systematically. Phonon dispersion relation, three phonon scattering, and the maximum mean-free-path are evaluated according to the results, which ultimately provide a theoretical guidance for  $\alpha$ - $\text{Ga}_2\text{O}_3$  material applications.

## II. MODELLING

### A. Microstructure and Brillouin zone

Corundum structure  $\alpha$ -phase  $\text{Ga}_2\text{O}_3$  has a  $R\bar{3}c$  crystal symmetry.<sup>31</sup> Distinguished from the monoclinic structure of  $\beta$ -phase  $\text{Ga}_2\text{O}_3$ , the rhombohedral corundum structure  $\alpha$ - $\text{Ga}_2\text{O}_3$  has an only octahedral coordinated  $\text{Ga}^{3+}$  ion, and two-thirds of the octahedral sites are hold by the  $\text{Ga}^{3+}$  ion,<sup>32</sup> while each Ga atom shared

one face and three edges with adjacent octahedra.<sup>31,32</sup> The oxygen atoms display close to the hexagonal arrangement.<sup>31,32</sup> In this study, conventional and primitive unit cell structures are visualized utilizing VESTA software,<sup>33</sup> as shown in Figs. 1(a) and 1(b)

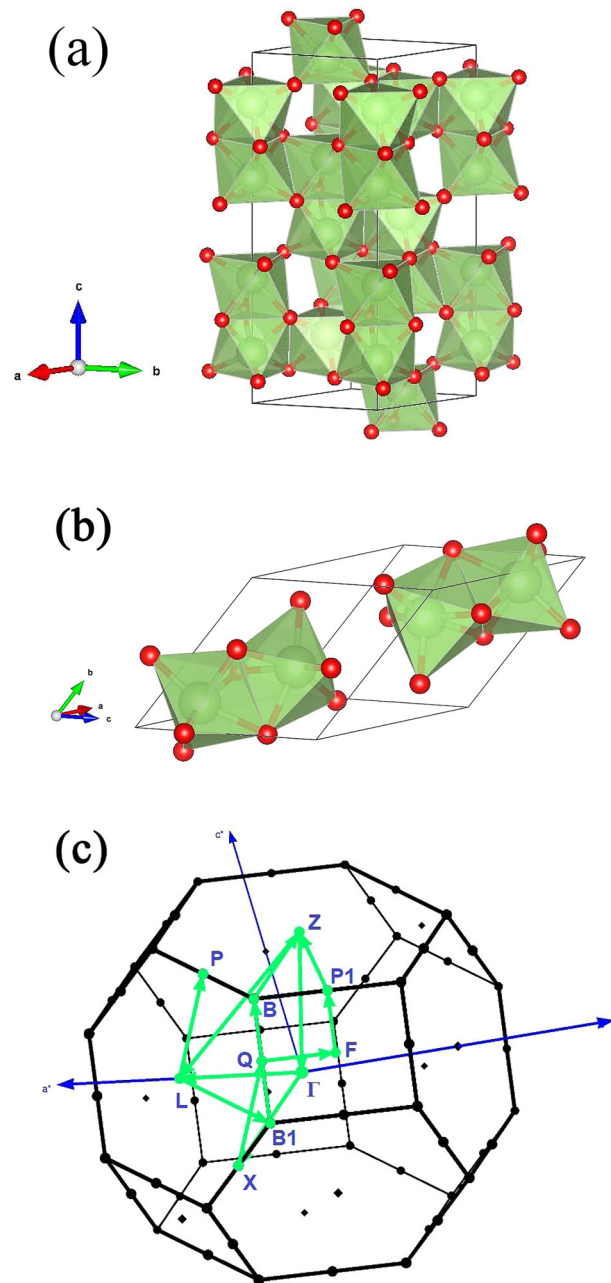


FIG. 1. Crystal structure and the Brillouin zone of  $\alpha$ - $\text{Ga}_2\text{O}_3$ , (a) conventional unit cell, (b) primitive unit cell, and (c) Brillouin zone and high symmetry k-paths. Large green ball corresponds to Ga atoms, while small red ball corresponds to O atoms.

Brillouin zone (BZ) and subsequent high symmetry directions are determined according to the method provided by Wahyu and Stefano *et al.*<sup>34</sup> For corundum structure  $\alpha$ -Ga<sub>2</sub>O<sub>3</sub>, the corresponding rhombohedral (RHL, hR)-type Brillouin zone and high symmetry k-point paths are selected in this study. Brillouin zone and high symmetry paths of  $\alpha$ -Ga<sub>2</sub>O<sub>3</sub> can also be visualized using XCrySDen software.<sup>35</sup> For the  $R\bar{3}c$  symmetry structure, the coordinates of symmetry points and the high symmetry paths in the first Brillouin zone are  $\Gamma$ -L-B<sub>1</sub>|B-Z- $\Gamma$ -X|Q-F-P<sub>1</sub>-Z|L-P, as illustrated in Fig. 1(c).

## B. Computational details

In this article, first-principles density functional calculations (DFT) are carried out using Quantum ESPRESSO software package.<sup>36,37</sup> Phonopy software package is used to compute harmonic phonon properties based on the finite displacement method.<sup>25</sup> The anharmonic force constant is calculated from the thirddorder.py code. Finally, the lattice thermal conductivity of  $\alpha$ -Ga<sub>2</sub>O<sub>3</sub> is obtained by solving the linearized phonon Boltzmann transport equation using an iterative procedure as implemented in ShengBTE software package.<sup>38,39</sup> As a comparison, we also calculate the lattice thermal conductivity of  $\beta$ -Ga<sub>2</sub>O<sub>3</sub> using the same method, and there is good agreement with experimental results.<sup>22</sup>

First of all, for the DFT calculations, the plane-wave-based algorithm and the projector-augmented wave method are employed together with Perdew–Burke–Ernzerhof exchange correlation functional. In order to make sure the structure steady, before implementing the plane wave self-consistent field calculation, we carry on a structure optimization procedure using the projector-augmented wave method with a generalized gradient approximation. We adopt the experimental lattice parameters as an initial data for performing the crystal structure optimization.<sup>6</sup> A plane wave cutoff of 125 Ry with a  $16 \times 16 \times 16$  k-point grids are used to relax the structure, and energy convergence criterion is set to be  $10^{-12}$  Ry. The structure is relaxed to force levels less than  $10^{-6}$  Ry/Bohr. The optimized structure parameters are applied to following calculations. For plane wave basis, we chose 125 Ry as energy cutoff for the wave functions and 500 Ry as energy cutoff for charge density and potential in the self-consistent field calculation. For better convergence, the system total energy convergence criterion is setup to be  $10^{-12}$  eV. We selected Ga.pbesol-dn-kjpaw\_psl.0.2.UPF and O.pbesol-n-kjpaw\_psl.0.1.UPF as implemented pseudopotentials files from Quantum ESPRESSO pseudopotentials library.<sup>36,37</sup> Phonon dynamics properties are investigated based on the density functional perturbation theory.<sup>40</sup> Born effective charges and dielectric tensor are obtained from the phonon dynamics calculation. Longitudinal and transverse optical phonon (LO-TO) splitting at the  $\Gamma$  point is also examined in this study.

The phonon dispersion curve and projected density of states of  $\alpha$ -Ga<sub>2</sub>O<sub>3</sub> are obtained from self-consistent energy calculations using software Phonopy interface with Quantum ESPRESSO package. We adopted a  $2 \times 2 \times 2$  supercell structure, and each supercell structure includes 80 atoms. Five displaced supercell structures are constructed using Phonopy package where the BZ is sampled by  $4 \times 4 \times 4$  k-point grids. Second-order force constants (IFCs) are evaluated in combining Phonopy package with the Quantum ESPRESSO phonon dynamic calculation. The presence

of third-order anharmonic IFCs leads to the appearance of scattering as a result of three-phonon interactions, and their values were obtained in combining the self-consistent field calculation using thirddorder.py code with Quantum ESPRESSO package. Considering the third nearest-neighbor interaction, 152 supercell structure configurations are created and tested with thirddorder.py code. Self-constant energy calculation is implemented based on the created supercell structure using Quantum ESPRESSO package. For higher calculation efficiency while maintaining the computational precision, we use “K\_POINTS gamma” mesh instead of “K\_POINTS automatic” mesh in the first Brillouin zone when carrying self-consistent computation.

After we obtained the second-order force constants from Phonopy package and third-order force constant from thirddorder.py code, we can implement the ShengBTE package with a CONTROL input file. Born charges and dielectric tensor in the CONTROL file can be obtained from previous phonon dynamics calculation using Quantum ESPRESSO package. Running the ShengBTE code is very straightforward, and there is no other argument need to input.

## III. RESULTS AND DISCUSSION

### A. Phonon dispersion

The calculated phonon dispersion curves and the projected density of states of  $\alpha$ -Ga<sub>2</sub>O<sub>3</sub> are shown in Fig. 2.

It can be seen from Fig. 2 that the phonon frequency of  $\alpha$ -Ga<sub>2</sub>O<sub>3</sub> is in the range of 0–21 THz. The splitting of LO-TO phonons at the  $\Gamma$  point can also be observed, which is a typical feature for an ionic crystal structure. In addition, it also can be seen from projected densities of states in Fig. 2 that phonon modes with a lower frequency are mostly correlated to the larger mass Ga atoms, while phonon modes with a higher frequency are mainly relevant to small mass O atoms. In fact, O vacancies and substitutional impurities at O sites are the most common defects in Ga<sub>2</sub>O<sub>3</sub> materials. O vacancies can affect the phonon scattering process, thereby furthermore affect the lattice thermal conductivity of the

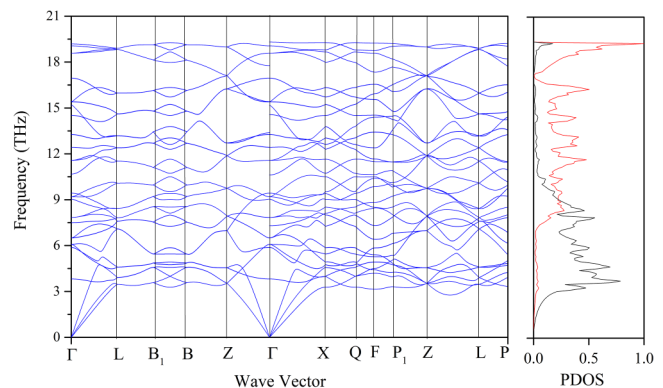


**FIG. 2.** Phonon dispersion curve and projected densities of states for  $\alpha$ -Ga<sub>2</sub>O<sub>3</sub>. Black curve corresponds to Ga atoms, while red curve corresponds to O atoms in the projected densities of states.

Ga<sub>2</sub>O<sub>3</sub> material.<sup>29</sup> For optoelectronic or other high-power electrical device applications, we can adjust the quantity of O vacancies or doping other elements in the O site to control the lattice thermal conductivity of α-Ga<sub>2</sub>O<sub>3</sub> materials.

## B. Thermal conductivity

After we obtain the harmonic and anharmonic interaction force constants, we can solve the linear form phonon Boltzmann transport equation. In this study, we adopted a directly iterative approach. The tensor form of lattice thermal conductivity can be described as<sup>28</sup>

$$K^{xy} = \frac{1}{V} \sum_{\lambda} c_{\lambda} v_{\lambda}^x v_{\lambda}^y \tau_{\lambda}, \quad (1)$$

where  $K$  is the lattice thermal conductivity;  $V$  is the unit cell;  $c_{\lambda}$  is specific heat capacity that is closely related to temperature;  $x$  and  $y$  are the Cartesian tensor coordinates;  $v_{\lambda}^x$  and  $v_{\lambda}^y$  are the phonon group velocities in  $x$  and  $y$  directions, respectively; and  $\tau_{\lambda}$  is the phonon relaxation time. In this study, we only consider an up to three-phonon scattering process. We implement a full iterative solution on lattice thermal conductivity for α-Ga<sub>2</sub>O<sub>3</sub> using ShengBTE package. It should be noted that Born effective charges and the dielectric tensor in the control file are setup according to phonon dynamics calculation results. Meanwhile, in order to obtain a full and steady numerical solution, we also tested different sample meshes; mesh density varies from 10 × 10 × 10 expanded up to 18 × 18 × 18. All test meshes reach a consistent convergence and the maximum error less than 0.5 Wm<sup>-1</sup> K<sup>-1</sup>, as the mesh size increases, the memory and calculated time will tremendously increase. Finally, considering a better convergence and computational time, we choose the mesh density 14 × 14 × 14 for the following lattice thermal conductivity calculation at various temperatures. The obtained lattice thermal conductivities of α-phase Ga<sub>2</sub>O<sub>3</sub> with various temperatures are shown in Fig. 3.

It can be seen from Fig. 3 that α-phase Ga<sub>2</sub>O<sub>3</sub> displayed a nearly isotropic thermal conductivity along three vector directions of the primitive cell. The maximum value of lattice thermal conductivity is found in the direction of [100], and the calculated value is 11.61 Wm<sup>-1</sup> K<sup>-1</sup> at room temperature. In contrast, the calculated lattice thermal conductivity of α-Ga<sub>2</sub>O<sub>3</sub> in the direction of [010] is 9.38 Wm<sup>-1</sup> K<sup>-1</sup> and in the direction of [001] is 8.94 Wm<sup>-1</sup> K<sup>-1</sup>, respectively. The minimum value of lattice thermal conductivity for α-Ga<sub>2</sub>O<sub>3</sub> is found in the direction of [001]. However, compared to β-phase Ga<sub>2</sub>O<sub>3</sub>, α-Ga<sub>2</sub>O<sub>3</sub> shows a lower thermal conductivity in a board temperature region from 30 to 800 K. At the same temperature, the maximum thermal conductivity of α-Ga<sub>2</sub>O<sub>3</sub> in the [100] direction is still lower than the minimum thermal conductivity of β-phase Ga<sub>2</sub>O<sub>3</sub> in the [100] direction (see Fig. 3). Compared with β-Ga<sub>2</sub>O<sub>3</sub>, the reduction in thermal conductivity of α-Ga<sub>2</sub>O<sub>3</sub> may be correlated to its unique microstructure. It also can be seen from Fig. 3 that the lattice thermal conductivity of α-phase Ga<sub>2</sub>O<sub>3</sub> decreased with increasing temperature in a broad temperature region from 30 to 800 K. In the low-temperature region (>30 K), lattice thermal conductivity of α-Ga<sub>2</sub>O<sub>3</sub> exhibited an exponential  $\kappa = \exp(\Theta/T)$  correlation with temperature.<sup>41</sup> However, in the

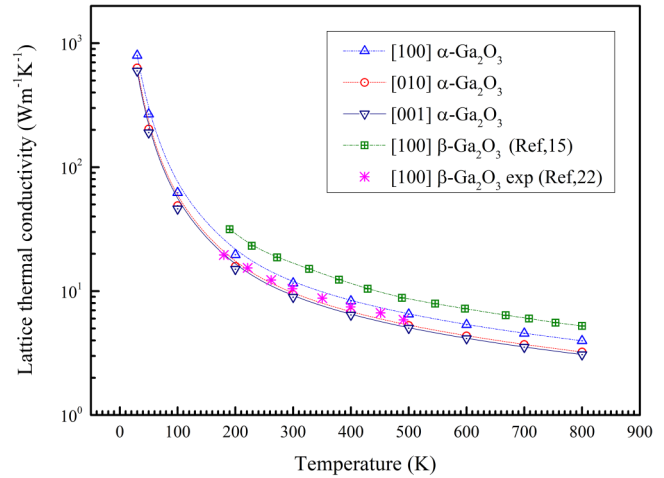


FIG. 3. Calculated lattice thermal conductivities of α-phase Ga<sub>2</sub>O<sub>3</sub> in function of temperature and thermal conductivities of β-phase Ga<sub>2</sub>O<sub>3</sub> from Refs. 15 and 22 shown for comparison.

high-temperature region, similar to β-phase Ga<sub>2</sub>O<sub>3</sub>, lattice thermal conductivity of α-phase Ga<sub>2</sub>O<sub>3</sub> also obeys T<sup>-1</sup> law with increasing temperatures, which implied that the Umklapp phonon scattering process occurred in this temperature region. It should be specially noted that the phonon scattering process is correlated to the microstructure. Referring to polymorphic Ga<sub>2</sub>O<sub>3</sub> materials, the phonon scattering process of α-phase Ga<sub>2</sub>O<sub>3</sub> is distinguished from common β-phase Ga<sub>2</sub>O<sub>3</sub>.

## C. Phonon scattering process

In order to explore the thermal transport mechanism of α-phase Ga<sub>2</sub>O<sub>3</sub> materials, we carefully examined the phonon scattering process. Three key parameters, i.e., the anharmonic scattering rate, the dimensionless scattering phase space volume, and weight phase space are studied. For further understanding the phonon thermal transport process, we first obtain the anharmonic scattering rate curve (inverse of scattering time) of α-phase Ga<sub>2</sub>O<sub>3</sub> at room temperature using ShengBTE package, and we compare the anharmonic scattering rate curve between α-phase and β-phase Ga<sub>2</sub>O<sub>3</sub>. The results are shown in Fig. 4.

It can be seen from Fig. 4 that the phonon anharmonic scattering rate of α-phase Ga<sub>2</sub>O<sub>3</sub> materials is clearly higher than β-phase Ga<sub>2</sub>O<sub>3</sub> in the entire frequency region. By comparing the microstructure of α and β-phase Ga<sub>2</sub>O<sub>3</sub>, it can be found that a higher phonon scattering rate of α-phase Ga<sub>2</sub>O<sub>3</sub> may root in its small primitive cell volume. In fact, corundum structure α-Ga<sub>2</sub>O<sub>3</sub> has the smallest unit cell volume of all the five polymorphs Ga<sub>2</sub>O<sub>3</sub> materials.<sup>42</sup> Besides, a higher phonon anharmonic scattering rate means that it has a small phonon relaxation time, which will lead to a significant reduction in lattice thermal conductivity. In fact, the anharmonic scattering process involves two effects, anharmonicity and scattering phase space.<sup>40</sup> Scattering phase space describe the three-phonon scattering process that obeys the momentum and

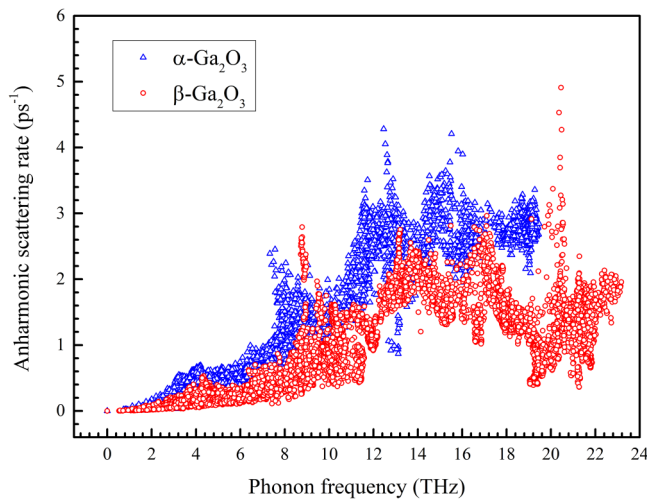


FIG. 4. Anharmonic scattering rate curve of  $\alpha$ -Ga<sub>2</sub>O<sub>3</sub>.

energy conservation law.<sup>43</sup> In order to explore the three-phonon scattering mechanism of  $\alpha$ -Ga<sub>2</sub>O<sub>3</sub>, we calculated another two key parameters, dimensionless scattering phase space volume  $P_3^j(q)$  and weighted phase space using the ShengBTE package,<sup>38</sup> and we compared these parameters with common  $\beta$ -Ga<sub>2</sub>O<sub>3</sub>. Dimensionless scattering phase space volume  $P_3^j(q)$  describes the volume in phase space for each mode and irreducible q point,<sup>15</sup> while weighted phase space describes the amount of three-phonon scattering process that obeyed momentum and energy conservation law.<sup>28,43</sup> The obtained results are shown in Fig. 5.

It can be observed from Fig. 5(a) that dimensionless scattering phase space volume decreases with increasing frequency for  $\alpha$ -phase Ga<sub>2</sub>O<sub>3</sub>. However, compared with  $\beta$ -phase Ga<sub>2</sub>O<sub>3</sub>, it can be found that  $\alpha$ -Ga<sub>2</sub>O<sub>3</sub> exhibits a small dimensionless scattering phase volume in the high-frequency region (>10 THz), while in the low-frequency region (<10 THz), it exhibits a larger value. These results probably correlate to the microstructure of  $\alpha$ -Ga<sub>2</sub>O<sub>3</sub>. As described previously,  $\alpha$ -Ga<sub>2</sub>O<sub>3</sub> has the smallest unit cell volume. Phonon scattering has more chance to occur, especially for the high frequency optical phonon. However, on the whole, the difference in dimensionless scattering phase volume between  $\alpha$  and  $\beta$ -phase Ga<sub>2</sub>O<sub>3</sub> is not evident.

As described in the literature,<sup>43</sup> weight phase space implied the amount of three-phonon scattering process that obeyed momentum and energy conservation law.<sup>28</sup> It can be seen from Fig. 5(b) that weight phase space of  $\alpha$ -phase Ga<sub>2</sub>O<sub>3</sub> is larger than  $\beta$ -phase Ga<sub>2</sub>O<sub>3</sub> in the high-frequency region (>10 THz). However, comprehensively, there is no significant difference in weight phase space between  $\alpha$  and  $\beta$ -phase Ga<sub>2</sub>O<sub>3</sub>. Therefore, combining with Figs. 4 and 5(b), we can conclude that the reduction in lattice thermal conductivity of  $\alpha$ -Ga<sub>2</sub>O<sub>3</sub> may be attributed to its strong anharmonic scattering process, it may be correlated to the microstructure, especially, it correlated with the band strength between the Ga and O atoms, as well as the mass differences between the Ga atoms and O atoms.

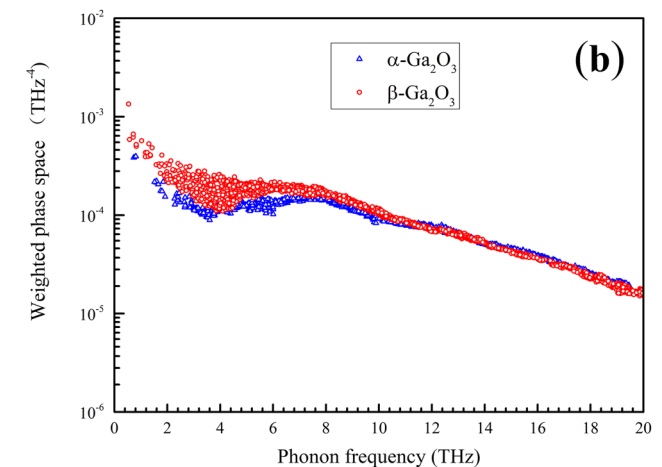
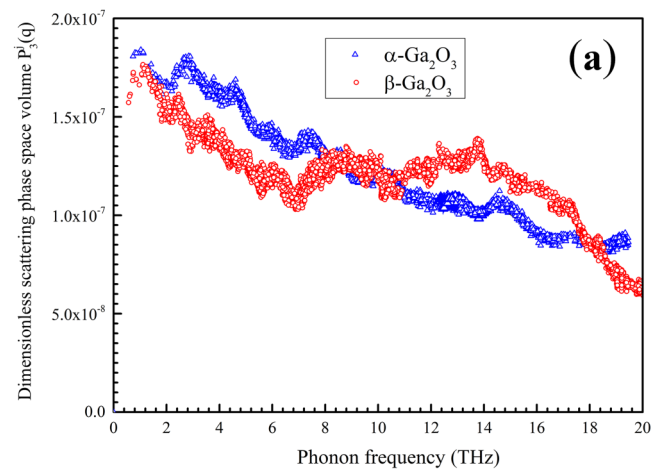


FIG. 5. Comparison on phonon scattering processes between  $\alpha$ - and  $\beta$ -Ga<sub>2</sub>O<sub>3</sub>: (a) dimensionless scattering phase space volume and (b) weighted phase space.

#### D. Phonon free mean path

For a real application of  $\alpha$ -Ga<sub>2</sub>O<sub>3</sub>, the active material is mostly used in a form of thin film where the size effect and interface effects may become significant. In addition, considering Ga<sub>2</sub>O<sub>3</sub>-based application in power devices, interface thermal resistance issue also needs to be addressed. One of the key parameters that determine the thermal transport for  $\alpha$ -Ga<sub>2</sub>O<sub>3</sub> thin film is the phonon mean free path. Therefore, a study on phonon mean-free path of  $\alpha$ -Ga<sub>2</sub>O<sub>3</sub> is important. In this article, we focused on the correlation between the thermal conductivity and the phonon mean-free path. The obtained cumulative thermal conductivities with various maximum free mean paths at different temperatures are shown in Fig. 6.

It can be seen from Fig. 6 that maximum mean free path decreased with increasing temperature. At lower temperatures,

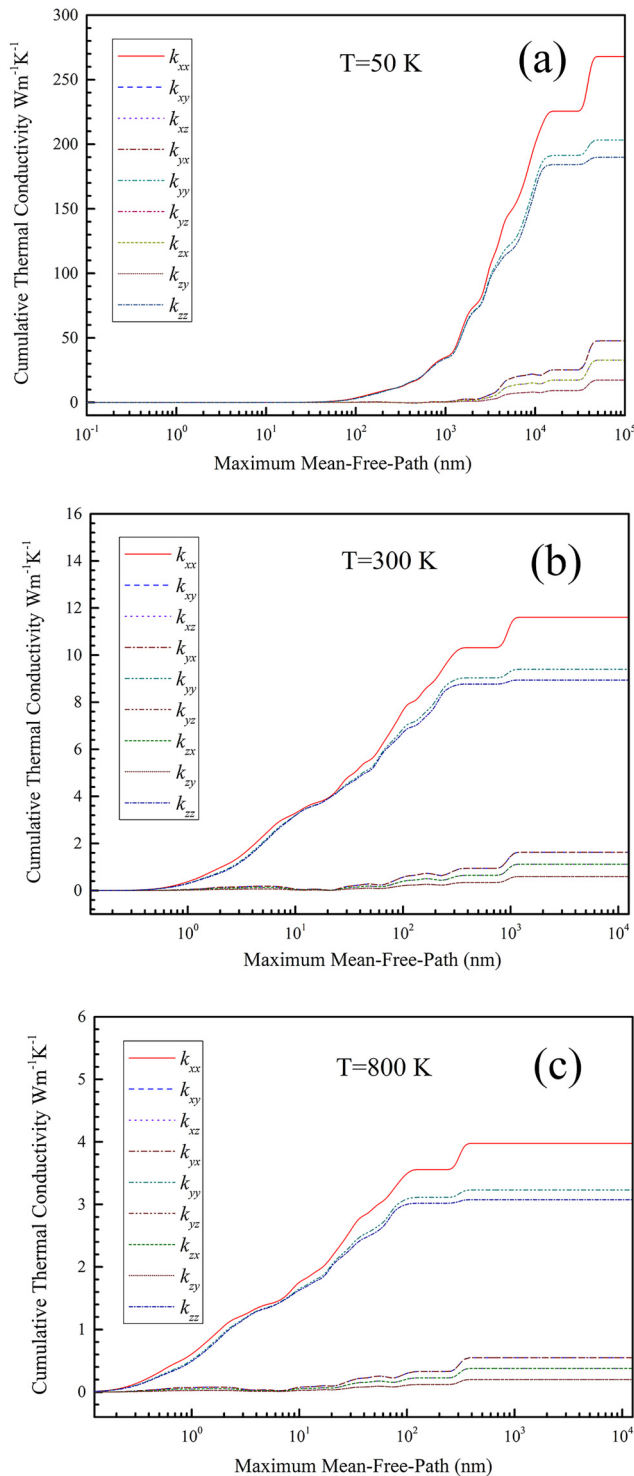


FIG. 6. Maximum mean-free-path at different temperature: (a) 50, (b) 300, and (c) 800 K.

50 K, the maximum mean free path is in a range of  $10^2$ – $10^5$  nm, and the thermal transport process is mainly decided by longitudinal phonon. At room temperature 300 K, the maximum mean free path is in a range of 10–1000 nm. Considering a low thermal conductivity of  $\text{Ga}_2\text{O}_3$  materials, one potential method to solve heat dissipation issue is to directly deposit  $\text{Ga}_2\text{O}_3$  on a high thermal conductivity substrate, such as other wide-bandgap semiconductor material diamond ( $>2000 \text{ Wm}^{-1} \text{ K}^{-1}$ ) or other high thermal conductivity semiconductor materials including boron arsenide (BAs) and boron phosphide (BP).<sup>44,45</sup> Therefore, phonon reflection or transmission behavior at interface will have a significant impact on the thermal transport process and it is closely correlated with the phonon mean free path. At high temperature, 800 K, the maximum mean free path is in range of 1–100 nm, so it is highly possible that the interface boundary scattering effects will influence the thermal transport process. Hence, considering  $\alpha$ - $\text{Ga}_2\text{O}_3$  materials for future power device applications, size and interface scattering effects need to be evaluated in detail.

#### IV. SUMMARY AND CONCLUSIONS

Based on first principles calculation and the iterative solution phonon Boltzmann transport equation, we investigated the lattice thermal conductivity of wide-bandgap  $\alpha$ - $\text{Ga}_2\text{O}_3$  materials. Our results indicated that  $\alpha$ - $\text{Ga}_2\text{O}_3$  exhibits a lower thermal conductivity compared with common  $\beta$ - $\text{Ga}_2\text{O}_3$ . At room temperature, 300 K, the calculated value of lattice thermal conductivity for  $\alpha$ - $\text{Ga}_2\text{O}_3$  is  $11.61 \text{ Wm}^{-1} \text{ K}^{-1}$  in the direction [100],  $9.38 \text{ Wm}^{-1} \text{ K}^{-1}$  in the direction [010], and  $8.94 \text{ Wm}^{-1} \text{ K}^{-1}$  in the direction [001], respectively; the maximum value is found in the direction [100] and the minimum value is found in the direction [001]. As the temperature increases, the difference in thermal conductivity along three directions is not evident, exhibiting a nearly isotropic property. Moreover, the results also reveal that low-frequency phonon modes are correlated to larger mass Ga atoms, while the high-frequency phonon modes are relevant to small mass O atoms.

Compared to common  $\beta$ - $\text{Ga}_2\text{O}_3$ , the reduction in thermal conductivity of  $\alpha$ - $\text{Ga}_2\text{O}_3$  may be correlated to bond strength in Ga and O atoms. Based on our first principle calculated, we found that  $\alpha$ - $\text{Ga}_2\text{O}_3$  has a larger phonon anharmonic scattering rate, which results in a reduction in the lattice thermal conductivity. Considering the future application of  $\alpha$ - $\text{Ga}_2\text{O}_3$  thin film in the power devices, we also investigated the key parameter for the interface thermal transport, which is the phonon maximum mean-free path. At room temperature, the maximum mean free path of  $\alpha$ - $\text{Ga}_2\text{O}_3$  is in the range of 10–1000 nm, the size and interface effects will have an important influence on the thermal transport in thin film-based electrical devices, and phonon interface scattering effects will play a crucial role in thermal transport for  $\alpha$ -phase  $\text{Ga}_2\text{O}_3$  thin films. The results presented here would help to gain a perspective on the phonon transport mechanism of  $\alpha$ - $\text{Ga}_2\text{O}_3$  and also provide a help in future application in  $\alpha$ - $\text{Ga}_2\text{O}_3$  materials.

#### ACKNOWLEDGMENT

The author gratefully acknowledges financial support from the China Scholarship Council for overseas research work (Grant No. CSC201808310305).

## AUTHOR DECLARATIONS

### Conflict of Interest

The authors have no conflicts to disclose.

### Author Contributions

**Gang Yang:** Formal analysis (equal); Investigation (equal); Methodology (equal); Software (equal). **Pedro Rojo Romeo:** Writing – original draft (equal); Writing – review and editing (equal). **Aleksandra Apostoluk:** Writing – original draft (equal); Writing – review and editing (equal). **Bertrand Vilquin:** Supervision (equal); Writing – original draft (equal); Writing – review and editing (equal).

### DATA AVAILABILITY

The data that support the findings of this study are available from the corresponding author upon reasonable request.

### REFERENCES

- <sup>1</sup>J. Y. Tsao *et al.*, *Adv. Electron. Mater.* **4**, 1600501 (2018).
- <sup>2</sup>M. Higashiwaki and S. Fujita, *Gallium Oxide: Materials Properties, Crystal Growth, and Devices* (Springer Nature, Cham., 2020).
- <sup>3</sup>S. J. Pearton, F. Ren, and M. A. Mastro, *Gallium Oxide Technology, Devices and Applications*, edited by G. Korotcenkov (Elsevier, Amsterdam, 2018).
- <sup>4</sup>S. J. Pearton, J. Yang, P. H. Cary IV, F. Ren, J. Kim, M. J. Tadjer, and M. A. Mastro, *Appl. Phys. Rev.* **5**, 011301 (2018).
- <sup>5</sup>R. Roy, V. G. Hill, and E. F. Osborn, *J. Am. Chem. Soc.* **74**, 719 (1952).
- <sup>6</sup>J. W. Roberts, J. C. Jarman, D. N. Johnstone, P. A. Midgley, P. R. Chalker, R. A. Oliver, and F. C.-P. Massabuau, *J. Cryst. Growth* **487**, 23 (2018).
- <sup>7</sup>D. Shinohara and S. Fujita, *Jpn. J. Appl. Phys.* **47**, 7311 (2008).
- <sup>8</sup>Y. Cheng, Y. Xu, Z. Li, and J. Zhang, *J. Alloys Compd.* **831**, 154776 (2020).
- <sup>9</sup>K. Uno, M. Ohta, and I. Tanaka, *Appl. Phys. Lett.* **117**, 052106 (2020).
- <sup>10</sup>Y. Yao, S. Okur, L. A. M. Lyle, G. S. Tompa, T. Salagaj, N. Sbrockey, R. F. Davis, and L. M. Porter, *Mater. Res. Lett.* **6**, 268 (2018).
- <sup>11</sup>J. W. Roberts *et al.*, *J. Cryst. Growth* **528**, 125254 (2019).
- <sup>12</sup>A. Barthel *et al.*, *Micromachines* **11**, 1128 (2020).
- <sup>13</sup>F. Massabuau, D. Nicol, F. Adams, J. Jarman, J. Roberts, A. Kovács, P. Chalker, and R. Oliver, *J. Phys. D: Appl. Phys.* **54**, 384001 (2021).
- <sup>14</sup>D. Y. Guo, X. L. Zhao, Y. S. Zhi, and W. Cui, *Mater. Lett.* **164**, 364 (2016).
- <sup>15</sup>M. D. Santia, N. Tandon, and J. D. Albrecht, *Appl. Phys. Lett.* **107**, 041907 (2015).
- <sup>16</sup>L. L. Snead, T. Nozawa, Y. Katoh, T.-S. Byun, S. Kondo, and D. A. Petti, *J. Nucl. Mater.* **371**, 329 (2007).
- <sup>17</sup>A. Jeżowski, B. A. Danilchenko, M. Boćkowski, and I. Grzegory, *Solid State Commun.* **128**, 69 (2003).
- <sup>18</sup>K. Z. B. Chatterjee, C. D. Nordquist, U. Singiseti, and S. Choi, *IEEE Trans. Compon.* **9**, 2352 (2019).
- <sup>19</sup>H. Akazawa, *Vacuum* **123**, 8 (2016).
- <sup>20</sup>M. Handweg, R. Mitdank, Z. Galazka, and S. F. Fischer, *Semicond. Sci. Technol.* **31**, 125006 (2016).
- <sup>21</sup>M. Handweg, R. Mitdank, Z. Galazka, and S. F. Fischer, *Semicond. Sci. Technol.* **30**, 024006 (2015).
- <sup>22</sup>Z. Guo *et al.*, *Appl. Phys. Lett.* **106**, 111909 (2015).
- <sup>23</sup>Y. Zheng, E. Swinnich, and J.-H. Seo, *ECS J. Solid State Sci. Technol.* **9**, 055007 (2020).
- <sup>24</sup>Y. Zhang, Q. Su, J. Zhu, S. Koirala, S. J. Koester, and X. Wang, *Appl. Phys. Lett.* **116**, 202101 (2020).
- <sup>25</sup>A. Togo and I. Tanaka, *Scr. Mater.* **108**, 1 (2015).
- <sup>26</sup>K. Esfarjani and H. T. Stokes, *Phys. Rev. B* **77**, 144112 (2008).
- <sup>27</sup>B. Liu, M. Gu, and X. Liu, *Appl. Phys. Lett.* **91**, 172102 (2007).
- <sup>28</sup>S. Mu, H. Peelaers, and C. G. Van de Walle, *Appl. Phys. Lett.* **115**, 242103 (2019).
- <sup>29</sup>Z. Yan and S. Kumar, *Phys. Chem. Chem. Phys.* **20**, 29236 (2018).
- <sup>30</sup>E. Ahmadi and Y. Oshima, *J. Appl. Phys.* **126**, 160901 (2019).
- <sup>31</sup>H. He, R. Orlando, M. A. Blanco, R. Pandey, E. Amzallag, I. Baraille, and M. Rérat, *Phys. Rev. B* **74**, 195123 (2006).
- <sup>32</sup>A. Dulda, *Adv. Mater. Sci. Eng.* **2016**, 1.
- <sup>33</sup>K. Momma and F. Izumi, *J. Appl. Crystallogr.* **44**, 1272 (2011).
- <sup>34</sup>W. Setyawan and S. Curtarolo, *Comput. Mater. Sci.* **49**, 299 (2010).
- <sup>35</sup>A. Kokalj, *J. Mol. Graph. Model.* **17**, 176 (1999).
- <sup>36</sup>P. Giannozzi *et al.*, *J. Phys.: Condens. Matter* **21**, 395502 (2009).
- <sup>37</sup>P. Giannozzi *et al.*, *J. Phys.: Condens. Matter* **29**, 465901 (2017).
- <sup>38</sup>W. Li, J. Carrete, N. A. Katcho, and N. Mingo, *Comput. Phys. Commun.* **185**, 1747 (2014).
- <sup>39</sup>W. Li, L. Lindsay, D. A. Broido, Derek A. Stewart, and Natalio Mingo, *Phys. Rev. B* **86**, 174307 (2012).
- <sup>40</sup>S. D. G. S. Baroni, A. Dal Corso, and P. Giannozzi, *Rev. Mod. Phys.* **73**, 515 (2001).
- <sup>41</sup>T. M. Tritt, *Thermal Conductivity Theory, Properties, and Applications*, Physics of Solids and Liquids Series (Springer, Boston, MA, 2004).
- <sup>42</sup>J. E. N. Swallow *et al.*, *Chem. Mater.* **32**, 8460 (2020).
- <sup>43</sup>W. Li and N. Mingo, *Phys. Rev. B* **91**, 144304 (2015).
- <sup>44</sup>Z. Cheng, F. W. Mu, L. Yates, T. Suga, and S. Graham, *ACS Appl. Mater. Interfaces* **12**, 8376 (2020).
- <sup>45</sup>J. S. Kang, M. Li, H. Wu, H. Nguyen, T. Aoki, and Y. J. Hu, *Nat. Electron.* **4**, 416 (2021).